nature

SUPPLEMENTARY INFORMATION

https://doi.org/10.1038/s41586-019-1581-9

In the format provided by the authors and unedited.

Low-barrier hydrogen bonds in enzyme cooperativity

Shaobo Dai[1,2,4], Lisa-Marie Funk[1,2,4], Fabian Rabe von Pappenheim[1,2], Viktor Sautner[1,2], Mirko Paulikat[3], Benjamin Schröder[3], Jon Uranga[3], Ricardo A. Mata[3]* & Kai Tittmann[1,2]*

[1]Department of Molecular Enzymology, Göttingen Centre for Molecular Biosciences and Albrecht-von-Haller Institute, Georg-August University Göttingen, Göttingen, Germany. [2]Department of Structural Dynamics, Max-Planck-Institute for Biophysical Chemistry Göttingen, Göttingen, Germany. [3]Institute of Physical Chemistry, Georg-August University Göttingen, Göttingen, Germany. [4]These authors contributed equally: Shaobo Dai, Lisa-Marie Funk. *e-mail: rmata@gwdg.de; ktittma@gwdg.de

Supplementary Information

Low-barrier hydrogen bonds in enzyme cooperativity

Shaobo Dai [1,2 #], Lisa-Marie Funk [1,2 #], Fabian Rabe von Pappenheim [1,2],Viktor Sautner [1,2], Mirko Paulikat [3], Benjamin Schröder [3], Jon Uranga [3], Ricardo A. Mata [3, *], and Kai Tittmann [1,2, *]

[1] Dept. of Molecular Enzymology, Göttingen Centre for Molecular Biosciences and Albrecht-von-Haller Institute, Georg-August University Göttingen, Julia-Lermontowa-Weg 3, D-37077 Göttingen, Germany

[2] Dept. of Structural Dynamics, Max-Planck-Institute for Biophysical Chemistry Göttingen, Am Fassberg 11, D-37077 Göttingen, Germany

[3] Dept. of Computational Chemistry and Biochemistry, Institute for Physical Chemistry, Georg-August University Göttingen, Tammannstr. 6, D-37077 Göttingen, Germany

[#] Both authors contributed equally to this work.

* Corresponding authors. Email: ktittma@gwdg.de (K.T.), rmata@gwdg.de (R.A.M.)

Supplementary Results

Kinetic and structural analyses of human transketolase pseudo-phosphorylation variant T382E and variant T382Q

Although our structural and functional analysis of the human transketolase wire variant E160Q indicated that cooperativity is linked to the LBHB between E366 and E160, one could argue that the E160Q variant not only disrupts the LBHB, but also changes the acid/base chemistry and charge situation directly next to the active site. In order to more categorically demonstrate the role of the wire and of the LBHB in cooperativity and catalysis, one would require a small perturbation of the LBHB, while keeping the chemical identity and mechanics of the wire intact. It is known that the activity of human transketolase is regulated by reversible phosphorylation of residue Thr382 [27]. Specifically, phosphorylation of Thr382 leads to a multifold increase of the enzymatic activity of human transketolase. Thr382 is located on the surface of the protein, more than 20 Å away from the active sites and the proton wire (Extended Data Fig. 4d). It contacts, however, the helix bearing residue E366. As outlined before, E366 is required for cofactor activation and forms an LBHB with E160 as part of the wire, thus it is central to the proposed cooperativity pathway. Therefore, the phosphorylation of Thr382 offers a unique opportunity to study both the impact of distant modifications on the proton wire and their contributions toward cooperativity and LBHBs, in particular because it is biologically relevant and not artificial. We thus generated a ‘pseudo-phosphorylation‘ variant, in which T382 had been replaced by a glutamate, and thus mimics phosphorylation. We then studied the kinetics and thermodynamic properties of the T382E ’pseudo-phosphorylation‘ variant (Extended Data Fig. 4a-c, Extended Data Table 2a). This variant exhibits an almost two-fold increased enzymatic activity compared to the wild-type enzyme in line with earlier studies [27]. In addition to the steady-state kinetic analysis, we examined the transient kinetics of substrate binding by stopped-flow to assess the degree of cooperativity and the microscopic rate constants of substrate binding in the variant (Extended Data Fig. 4b, Extended Data Table 2a). Intriguingly, variant T382E exhibits an enhanced positive cooperativity with an estimated Hill coefficient of n_H = 2.42 ± 0.36 (the non-phosphorylated form of human transketolase exhibits a milder positive cooperativity with n_H = 1.56 ± 0.25). Also, the substrate equilibrium binding constant $K_{0.5}$ is three-fold decreased relative to the wild-type indicating a more efficient initial binding along with a faster formation of the covalent substrate-ThDP conjugate ($k_{forward}$, Extended Data Table 2a). Next, we studied the thermodynamic properties of the proton wire in variant T382E by assessing the p*K*a of the ThDP-E366‘ proton shuttle using CD spectroscopy (Extended Data Fig. 4c, Extended Data Table 2a). For the variant, the p*K*a has shifted from 5.79 ± 0.03 (non-phosphorylated wild-type) to 5.17 ± 0.02. This showcases that (pseudo-) phosphorylation of human transketolase at position T382 impacts the properties of the proton wire and activation apparatus. In variant

T382E, an evolving negative charge at E366 can be more effectively stabilized than in the non-phosphorylated wild-type. Conversely, a disengagement of the LBHB between E366 and E160 and the resultant disruption of the wire mechanics in the E160Q variant decreased the ability to stabilize the negative charge at E366 (higher p*K*a), and also resulted in a complete loss of cooperativity. In order to illuminate the structural basis for the enhanced activity and cooperativity of variant T382E, we crystallized this variant and determined its X-ray crystallographic structure at a resolution of 1.15 Å. Our structural analysis could confirm the introduced T→E mutation at position 382 and gave insights into structural changes of the proton wire (Extended Data Fig. 4e). While the positions of hydrogen atoms cannot be unambiguously traced at this resolution, the interatomic distances between amino acid residues, cofactor ThDP and water molecules can be quantified with high accuracy. The X-ray structure reveals that the side-chain of E382 now points to the outside contrasting the observation for wild-type transketolase, where T382 points to the inside (Extended Data Fig. 4d). The most remarkable observation, however, is the further compression of the LBHB interaction between E366‘ and E160 from 2.56 Å (wild-type) to 2.52 Å in the ‘pseudo-phosphorylation‘ variant T382E along with a minute change for the distance between E366‘ and ThDP-N1‘. In addition to the T382E ‘pseudo-phosphorylation‘ variant, we generated an isosteric T382Q variant in order to discriminate between the impact of charge and of sterics. Variant T382Q exhibits a markedly reduced enzymatic activity (10% residual activity relative to wild-type) with negative cooperativity (Hill coefficient n_H = 0.80 ± 0.04, Extended Data Table 2a). Also, this variant partially loses its cofactor ThDP rationalizing the impaired activity and suggesting a disruption of the wire. As variant T382Q is not stable enough to allow crystallization, we do not have an atomic structure in that case, but the functional data showcases that phosphorylation residue 382 is critically controlling the function of the proton wire including the LBHB through subtle repositioning of E366.

All in all, the functional and structural studies of human transketolase variants with changes of phosphorylation site T382 and wire residue E160 pinpoint a critical role of the wire, in particular of the LBHB between E366 and E160, for cooperativity and active site synchronization. A further compression of the LBHB in variant T382E leads to an enhanced positive cooperativity and higher enzymatic activity, while the disengagement of the LBHB in variant E160Q results in a loss of cooperativity and reduced activity. Likewise, variant T382Q, where the wire seems to be mechanically disrupted as evidenced by the partial loss of cofactor ThDP, exhibits negative cooperativity and greatly reduced enzymatic activity.

Kinetic analysis of pyruvate oxidase wild-type and variants

We comparatively analyzed the steady-state and pre-steady-state kinetics of POX wild-type versus mutant proteins, in which wire residues engaged in LBHBs (E59', H89', E60) were replaced by site-directed mutagenesis (see Fig. 3 main manuscript and SI Methods).

Steady-state kinetic analysis

An isosteric substitution of E59' by glutamine almost completely abolishes catalysis when using an artificial redox assay in which 2,6-dichlorophenolindophenol replaces oxygen as final electron acceptor (Extended Data Table 2b). Inasmuch the observed LBHB of E59' with ThDP-N1' contributes to catalysis remains ambiguous as E59' is also acting as a bona fide acid-base catalyst required for cofactor activation. Mutations of residues H89' and E60, which are also interacting via a LBHB, are more insightful in this regard. All protein variants exhibit very little effect on catalysis (k_{cat}) but display impaired substrate binding (multifold elevated Michaelis constants) (Extended Data Table 2b).

Pre-steady-state kinetic analysis

Using a specific stopped-flow based substrate binding assay, the *on*- and *off*-rate constants of the substrate was assessed (Extended Data Fig. 8a, b). The H89' and E60 variants exhibit 10 to 20-fold reduced second-order rate constants of substrate binding compared to the wild-type enzyme, while the off-rate is virtually unchanged (Extended Data Table 2b). Finally, we analyzed substrate binding and processing under single turnover conditions using the FAD cofactor as a spectroscopic probe (Extended Data Fig. 8c-f). Pyruvate oxidase wild-type displays positive cooperativity with a Hill factor n_H = 1.7, similar to our observations made for human transketolase wild-type. Remarkably, all pyruvate oxidase variants with isosteric substitutions of residues forming LBHBs (E59Q, H89N, E60Q) exhibit no cooperativity corroborating our hypothesis that the detected LBHBs in the communication proton wire are critical elements of the cooperativity pathway between the two remote active sites in the functional dimer. In terms of catalysis, the variants show different effects relative to the wild-type enzyme. While mutant protein E59Q is severely impaired due to the functional knock-out of cofactor activation, variants with substitutions at H89' or E60 are not defective in catalysis (Extended Data Table 2b). However, the pre-equilibrium binding of substrate is weakened (multifold increased substrate binding constant K_S^{app}).

In sum, the impact of the detected LBHBs in POX on catalysis is relatively small but they are functionally essential for cooperativity and active site synchronization between the remote active sites in the functional dimer, akin to the observations made for transketolase.

Supplementary Methods

Functional analysis of enzymes

1. Human transketolase

Steady-state kinetic analysis
The enzymatic activity of human transketolase was determined for the conversion of substrates *D*-xylulose-5-phosphate (X5P, donor) and *D*-ribose-5-phosphate (R5P, acceptor) into products sedoheptulose-7-phosphate (S7P) and glyceraldehyde-3-phosphate (G3P) in a spectrophotometric steady-state assay using auxiliary enzymes triose phosphate isomerase and *sn*-glycerol-3-phosphate : NAD + 2-oxidoreductase [24].

$$X5P + R5P \Leftrightarrow S7P + G3P \quad (1)$$

This assay detects formation of product G3P, which derives from cleavage of X5P. The concomitant oxidation of co-substrate NADH was monitored spectrophotometrically at 340 nm in 50 mM glycyl-glycine buffer, pH 7.6, at 20 °C. The assay contained 0.22 mM NADH, 3.6 units of *sn*-glycerol-3-phosphate : NAD+ 2-oxidoreductase/triose-phosphate isomerase, 100 µm ThDP, 5 mM $CaCl_2$, 0.1 – 2 mg/mL human transketolase, varied concentrations of donor substrate X5P and 2 mM R5P. One unit is defined as the formation of 1 µmol of G3P/min. The dependence of the initial rates on the substrate (X5P) concentration was analyzed according to the Michaelis-Menten equation (eq 2).

$$v(S) = \frac{V_{max} \cdot [S]}{K_M + [S]} \quad (2)$$

Analysis of Reaction Intermediates under Equilibrium Conditions by ^{1}H NMR Spectroscopy after Acid Quench Isolation
The reaction of human transketolase with donor substrate F6P was analyzed by 1D ^{1}H NMR spectroscopy after acid-quench isolation of reaction intermediates as reported before [24]. This assay permits the quantitative analysis of microscopic equilibria and key reaction intermediates of the donor half-reaction comprising the formation *i*) of the noncovalent enzyme : substrate Michaelis complex (K_1), *ii*) of the covalent F6P-ThDP conjugate (K_2), and the cleavage of the latter into the dihydroxyethyl-ThDP (DHEThDP) carbanion-enamine and product E4P (K_3).

$$\text{E-ThDP + F6P} \overset{K_1}{\Leftrightarrow} \text{E-ThDP : F6P (Michaelis complex)} \overset{K_2}{\Leftrightarrow} \text{E-F6P-ThDP} \overset{K_3}{\Leftrightarrow} \text{E-DHEThDP + E4P} \quad (3)$$

The concentrations of the intermediates were estimated by 1D ^{1}H NMR spectroscopy using the C2-H proton signal of C2-unsubstituted ThDP (9.70 ppm) and the C6′-H proton signals of chemically synthesized DHEThDP (7.31 ppm), and of chemoenzymatically synthesized F6P-ThDP (7.34 ppm) adducts as standards [43]. In a typical experiment, 15 mg/ml holoenzyme (219 µm active sites) in 50 mM glycyl-glycine, pH 7.6, was mixed with 100 mM F6P (in the

same buffer) in a 1 + 1 mixing ratio (200 µl each) for 30 s at 20 °C. The reaction was stopped by the addition of 200 µl of TCA/HCl as detailed in [43]. NMR data acquisition and processing were carried out as described previously [43].

Analysis of Protonic and Tautomeric Equilibria of Enzyme-bound Cofactor by CD Spectroscopy

The co-catalytically active aminopyrimidine moiety of bound cofactor ThDP adopts several distinct chemical states, each of which having a characteristic spectroscopic signature in circular dichroism (CD) spectroscopy [44, 45]. Model studies suggested that the aminopyrimidine form (AP) of ThDP exhibits a CD band at ~330 nm with negative signature, while the iminotautomer (iminopyrimidine, IP) shows a positive band at ~300 nm. Quantum-chemical calculations along with spectroscopic analysis of ThDP enzymes indicated that the AP band at 330 nm reports on the ionization state of the canonical glutamate residue that activates the ThDP cofactor (E366 in human transketolase) [46]. When the canonical Glu is ionized (negatively charged), the AP band is centered around 330 nm; when it is protonated (charge neutral) or replaced by a neutral residue such as a glutamine, the band shifts to ~285-290 nm [46].
In order to study the intrinsic protonic and tautomeric equilibria of ThDP bound to human transketolase, we collected near-UV CD spectra of the enzyme in pH titration experiments (Chirascan, Applied Photophysics, UK). In a typical experiment, 2 mg/ml enzyme in 20 mM glycyl-glycine/20 mM MES with a pH ~4.8 was gently titrated with Tris base (1 M, pH 11) until a basic pH of 9. CD spectra were recorded at each pH value between 250 and 400 nm at 20 °C with an optical pathlength of 10 mm. The apparent p*K*a of the cofactor-E366 proton shuttle was analyzed using the CD signal of the cofactor AP band at 330 nm and eq 4:

$$\Theta_{330}(pH) = offset + \frac{A}{1+10^{(pK_A - pH)}} \qquad (4)$$

In case of variant E160A two pH-dependent limbs were observed. Data were accordingly fitted with eq 5:

$$\Theta_{330}(pH) = offset + \frac{A_1}{1+10^{(pK_A{}^1 - pH)}} + \frac{A_2}{1+10^{(pK_A{}^2 - pH)}} \qquad (5)$$

Transient kinetics of substrate binding using stopped-flow

Substrate binding to transketolase was analyzed by stopped-flow kinetics (SX 20, Applied Photophysics, UK) using the UV-Vis signal of the enzyme-bound ThDP in its AP form at 325 nm as a spectroscopic reporter. Covalent binding of substrate F6P to ThDP goes along with a depletion of the cofactor AP band. 4 mg/ml human transketolase (wild-type and variants) were mixed with varied concentrations of substrate F6P in 5 mM $CaCl_2$, 50 mM glycyl-glycine pH 7.6 in a 1+1 mixing ratio at 4 °C. The reaction was monitored at 325 nm using an optical pathlength of 10 mm.
The monophasic signal decrease observed for the wild-type enzyme was fitted with a monoexponential function (eq 6)

$$A_{325}(t) = A_{325}{}^{0} + A \cdot e^{(-k_{app} \cdot t)} \quad (6),$$

where k_{app} denotes the apparent rate constant of formation of the covalent F6P-ThDP intermediate on the enzyme (see scheme below).

The biphasic signal change observed for transketolase variants was fitted with a double exponential function (eq 7)

$$A_{325}(t) = A_{325}{}^{0} + A_1 \cdot (1 - e^{(-k_{app1} \cdot t)}) + A_2 \cdot e^{(-k_{app2} \cdot t)} \quad (7),$$

where k_{app1} denotes the apparent rate constant of formation of the Michaelis complex and k_{app2} the apparent rate constant of formation of the covalent F6P-ThDP intermediate on the enzyme (see scheme below).

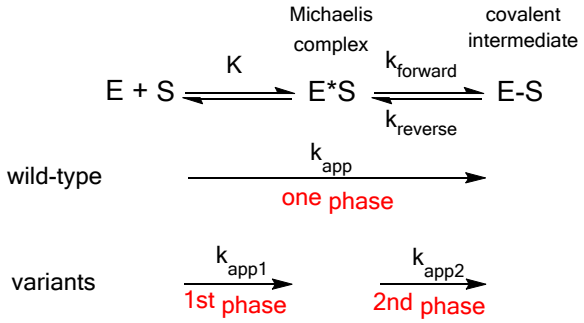

In view of the sigmoidal dependence of the rate constants with a non-zero y-intercept, the dependence of k_{app} (wild-type) and k_{app2} (variants) from the substrate concentration was analyzed using equation 8, which accounts for a two-step reversible binding mechanism (see scheme above) with cooperative binding

$$k_{app}(S) = k_{reverse} + \frac{k_{forward} \cdot [S]^n}{K_{0.5}{}^n + [S]^n} \quad (8)$$

where $k_{reverse}$ denotes the first-order rate constant of substrate elimination from the covalent substrate-cofactor (F6P-ThDP) intermediate (E-S in the scheme above), $k_{forward}$ the first-order rate constant of formation of the covalent substrate-cofactor (F6P-ThDP) intermediate, $K_{0.5}$ the dissociation constant of the preceding binding equilibrium between the resting-state enzyme and the enzyme : substrate Michaelis complex (E*S in the scheme above), and *n* the Hill coefficient as a measure of cooperativity.

T-jump kinetics

Relaxation kinetics of human transketolase in the resting state were measured after a T-jump from 12 °C to 20 °C using the TJ-64 instrument from TgK Scientific (Bradford-on-Avon, UK). A concentration of 5 mg/ml transketolase in 50 mM glycyl-glycine, pH 7.6 supplemented with 5 mM Ca^{2+} were placed in the sample cell, absorbance changes following the T-jump were monitored at 325 nm (absorbance band of the AP form of enzyme-bound ThDP) and at 294 nm (absorbance band of the IP form of enzyme-bound ThDP). A total of 50 transients were averaged in each case, the resultant average-transients were fitted with a monoexponential (325 nm, eq 6) or double exponential (294 nm, eq 7) function (see Extended Data Fig. 3).

2. Pyruvate oxidase

Steady-state kinetic analysis

The enzymatic activity of *L. plantarum* POX was measured with a spectrophotometric assay using the redox dye 2,6-dichlorophenolindophenol (DCPIP) as artificial electron acceptor [47]. DCPIP exhibits a blue colour in the oxidized state (λ_{max} ~600 nm, $\varepsilon_{600\ nm}$ = 17700 M^{-1} cm^{-1}) and becomes colourless upon POX-catalyzed two-electron reduction. Activity assays contained 200 mM potassium phosphate buffer pH 6.0, 100 µM ThDP, 1 mM $MgSO_4$, 100 µM DCPIP, 1-50 µg/mL POX and varied concentrations of substrate pyruvate (0-75 mM for wild-type and variants E60Q, E60A, H89N and H89A; 0-2.5 M for variant E59Q). Kinetic analysis were conducted at 600 nm with an optical pathlength of 10 mm at 25 °C. One unit is defined as the depletion of 1 µmol of DCPIP/min. The dependence of the initial rates on the substrate (pyruvate) concentration was analyzed according to the Michaelis-Menten equation (eq 2, see above).

Transient kinetics of substrate binding using stopped-flow

Kinetics of substrate binding was analyzed by UV-Vis stopped-flow experiments (SX 20, Applied Photophysics, UK) using the pyruvate analog methyl acetylphosphonate (MAP) [48, 49]. This analog binds covalently to enzyme-bound ThDP in pyruvate oxidase but is not further processed allowing to exclusively monitor substrate binding. POX wild-type and variants at a concentration of 2.5 mg/mL in 200 mM potassium phosphate buffer pH 6.0, 100 µM ThDP and 1 mM $MgSO_4$ were mixed with varied concentrations of MAP in the same buffer in 1+1 mixing ratio at 25 °C. Reaction was observed at 310 nm and using an optical pathlength of 10 mM.

The monophasic transients were fitted with a monoexponential function (eq 9)

$$A_{310}(t) = A_{310}{}^{0} + A \cdot e^{(-k_{app} \cdot t)} \qquad (9)$$

where k_{app} denotes the pseudo-first-order rate constant of formation of the covalent conjugate between MAP and enzyme-bound ThDP.

The linear dependence of k_{app} from the substrate analog concentration accounts for a two-state equilibrium

$$E + S \underset{k_{off}}{\overset{k_{on}}{\rightleftharpoons}} \underset{\text{covalent intermediate}}{E\text{-}S}$$

And was fitted with eq 10

$$k_{app} = k_{off} + k_{on} \cdot [S] \qquad (10)$$

where k_{off} denotes the first-order rate constant of dissociation of the substrate analog from the covalent intermediate and k_{on} the second-order rate constant of substrate binding.

Transient kinetics of substrate binding and processing under single-turnover conditions using stopped-flow

The kinetics of substrate binding and processing was analyzed under single turnover conditions using anaerobic stopped-flow experiments (SX 20, Applied Photophysics, UK) as described before [50]. Under these conditions, processing of substrate pyruvate at the active site leads to the reduction of the FAD cofactor of POX (see scheme below). Kinetic analyses permit determination of the dissociation constant *K* of substrate binding (pyruvate), and a rate constant k_{app} of substrate processing at the active site comprising several microscopic steps.

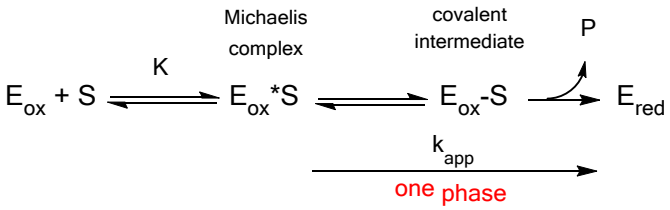

In a typical experiment, POX at a concentration of 3 mg/mL in 200 mM potassium phosphate buffer plus 100 µM ThDP, 1 mM $MgSO_4$ was mixed with varied concentrations of substrate pyruvate in a 1+1 mixing ratio under anaerobic conditions at 25 °C. The reaction was monitored at a wavelength of 457 nm, where the FAD cofactor in the oxidized state absorbs.

The monophasic transients were fitted with a monoexponential function (eq 11)

$$A_{457}(t) = A_{457}{}^{0} + A \cdot e^{(-k_{app} \cdot t)} \qquad (11)$$

where k_{app} denotes the apparent rate constant of pyruvate processing at the active site.

The sigmoidal dependence (with zero-y-intercept) from the applied pyruvate concentration was analyzed using equation 12, which accounts for a binding mechanism (see scheme above) with cooperative binding and at least one irreversible step of substrate processing

$$k_{app}(S) = \frac{k_{app}{}^{max} \cdot [S]^n}{K_{0.5}{}^{n} + [S]^n} \qquad (12)$$

where $k_{app}{}^{max}$ denotes the rate constant of substrate processing at substrate saturation, $K_{0.5}$ the dissociation constant of the preceding binding equilibrium between the resting-state enzyme and the enzyme : substrate Michaelis complex, and *n* the Hill coefficient as a measure of cooperativity.

Computational details

Molecular dynamics simulations

The human transketolase system was modeled based on the derived crystal structure. For the molecular dynamics (MD) simulations in solution, the ethylene glycol molecules and sodium ions were removed. The cofactors were taken and saturated with hydrogen atoms according to the X5P-ThDP-adduct state with the pyrimidine ring being in the imino form. An optimization at the B3LYP/def2-SVP level of theory followed [51, 52], constraining all dihedral angles in order to retain their conformations as in the protein pocket. Atomic charges were then determined with an electrostatic potential fit (HF/6-31G*). The remaining parameters were employed from the GAFF force field [53], while two new atom types were introduced for the C4' and N4' atoms of the iminopyrimidine ring as recently described [46]. The protein environment was parametrized with the Amber ff10 force field [54]. The protonation states of titratable residues were assigned either to information from the electron density map of the X-ray measurement or by inspection of their local environment. Notable exceptions from their reference states at a pH value of 7 are D424 interacting with the ThDP-bound substituent as well as H258 and H416, which are located in the proximity of the diphosphate moiety of ThDP and set doubly protonated (positively charged). The protonation states of the residues in the proton wire were chosen to be symmetric with the E366' residues set deprotonated (negatively charged) while the E160 and E165 residues being protonated (neutral). After addition of hydrogen atoms, the system charge of +8 (atomic units) was neutralized with chloride ions and placed into a TIP3P water box having a distance of 12 Å between the protein and the boundary of the box. A short minimization followed for the hydrogen atoms, chloride ions and water molecules. Here, the non-hydrogen atoms of the cofactors and the protein environment were restrained to their Cartesian positions with a harmonic potential employing a force constant of 5 kcal/mol/Å^2. This derived structure was taken as reference for the subsequent MD simulations and their analysis.

The system was then heated up in six stages over 60 ps to 300 K in a NVT simulation. For this and in the following simulations, periodic boundary conditions together with a cutoff of 12 Å for non-bonded interactions were applied. Furthermore, the SHAKE algorithm was employed to constrain bond lengths involving hydrogen atoms [55, 56], which additionally allowed the appli- cation of a time step of 2 fs. Constant temperature was achieved by usage of Langevin dynamics (collision frequency of 2 ps^{-1}). An equilibration phase followed for 500 ps in a NPT simulation, where isotropic position scaling was applied to achieve constant pressure (p = 1 bar). The root-mean-square-deviation of the protein backbone was here considered as convergence criterium. Afterward, the NPT simulation was extended for 16.5 ns as the final production phase. All MM calculations were carried out with the Amber 11 program package [57].

The MD simulations focused on the dynamics of the bridging water located at the glutamine bridge (as well as the two glutamines Q367). We wished to confirm whether or not an oscillating motion, bringing the water from one side of the proton wire to the other, could be observed. Furthermore, it was of interest to determine the time scale of these events. Structures were sampled in the production phase every 0.5 ps, and used for the analysis presented in SI Fig. 8. The results confirm the existence of this motion, with two clear regimes being identified. Visual inspection showed that these in fact overlap well with the partially occupied sites for both the water and the glutamines in the crystal structure data. A third regime was also observed between 4.0 and 10.2 ns, whereby the glutamine bridge moved out of position (high RMSD relative to the crystal structure). However, the system does return to the expected oscillatory behaviour at t > 10.2 ns. This means that although the simulation found a conformational space whereby the bridge is disconnected, the system can return to its former state. The structures outside of this time frame were analysed by a

density-based spatial clustering of applications with noise (DBSCAN) analysis [58], confirming the existence of two dominant conformations by the correlation between the water distance and the RMSD of the glutamines. The DBSCAN analysis was carried out with the sklearn module version 0.14.1 for Python, with epsilon=0.10 and min_samples = 30.

QM/MM calculations

The crystal structure of the wild-type human transketolase was employed in the QM/MM calculations. Since for these calculations we were interested in modelling the proton wire observed in the crystal, our preparation procedure was slightly different than in the MM calculations in order to ensure the crystal structure. H atoms were added to the structure and the minimization was carried out while restraining the non-H atoms with a larger force of 10 kcal/mol/Å^2. The steepest descendent algorithm was employed for the first 500 cycles and then 4500 cycles with conjugate gradient. The resulting structure was taken and a QM region was built consisting of E366', E160, E165 and a bridging water between E160 and E165. The residues were included up to the Cß atom, using then a link atom (hydrogen) along the Cß-Cα bond. Also, a QM proton was added to E165. The site used for the modelling was the one to the side where the shuttling water was located. Instead of simulating the proton shuttling by describing the two sites, the water and the proton were removed at one site. This is done through what is commonly called an "alchemical" transformation, meaning that the interactions to the system are gradually set to zero (effectively deleting the atoms). This was done in the proton case by scaling the nucleus charge (Z) by a parameter λ=1-0. At the same time, the well-depth of the Lennard-Jones potential (ε) and the charges of the MM water molecule were scaled by the same parameter. These atoms together with the MM environment were kept fixed during the optimizations. The scaling was performed following the formulae

$$q(i) = \lambda q(i)$$

$$\varepsilon(i) = 2\lambda\varepsilon(i); 0 < \lambda < 0.5$$

$$\varepsilon(i) = \varepsilon(i); \lambda \geq 0.5$$

For each value of λ (increments of 0.1 were used), the QM atom positions were optimized, while keeping the Cß atoms fixed. This resulted in the distances displayed on the left side of Fig. 2 in the main manuscript, detailing the hydrogen positions along the proton wire.
The QM/MM calculations were performed with Chemshell package [59]. The QM calculations were carried out with the ORCA 4.0.1 program package [60]. All geometry optimizations were done using Grimme's dispersion correction [61] with B3LYP [51] and the def2-SVP basis set [52]. Resolution of identity approximations were used employing the corresponding def2 auxiliary basis sets [62].
For the end points (λ=0 and λ=1) further scans were performed. The proton between E366' and E160 was placed in a straight line between the oxygens (O1 and O2), and single points were computed for different distances while keeping the rest of the system fixed. For each point in the scan DPLNO-CCSD(T) [63] energies were calculated, using the aug-cc-pVTZ basis set [64]. The DLPNO-CCSD(T) calculations were carried out with the RIJK approximation, with the default auxiliary basis sets.
The resulting one-dimensional scans were fit using a least squares approach with root mean square deviations of better than 0.3 kJ/mol. An 8th order polynomial expansion was employed:

$$V - V_{ref} = \sum C_i z^i \qquad (13)$$

where the internal coordinate z is defined as $z = {}^{1}/_{2}\,(\Delta R_{O1-H1} - \Delta R_{O2-H1})$ and $z = {}^{1}/_{2}\,(\Delta R_{O2-H1} - \Delta R_{O1-H1})$ for λ=1 and λ=0, respectively.

The potential energy curves were employed in variational calculations using an approximative vibrational Hamiltonian set up in normal coordinates:

$$\hat{H} = \frac{1}{2}\hat{P}^2 + V \qquad (14)$$

In eq 14 the momentum conjugate to the normal coordinate Q is given by $\hat{P} = -i\hbar\,{}^{\partial}/_{\partial Q}$ and V is the potential energy (as defined above). A matrix representation of the Hamiltonian was set up in a basis of 40 harmonic oscillator functions. Matrix elements of the Hamiltonian were calculated numerically by means of Gauss-Hermite integration. Evaluation of the potential energy involved a linear transformation from the normal to the internal coordinate $z = L \cdot Q$. The transformation coefficient was obtained by solving the harmonic problem of a proton moving in the harmonic potential

$V_{harm} = {}^{1}/_{2}\,F \cdot z^2$

by means of the standard Wilson GF method where

$G = {}^{1}/_{m_H}$ and $F = 2C_2$ (cf. eq 13).

Vibrational wavefunctions were thus obtained by diagonalizing the Hamiltonian and the corresponding distributions evaluated.